Korean J. Chem. Eng., 37(8), 1340-1345 (2020)
DOI: 10.1007/s11814-020-0617-z

pISSN: 0256-1115
eISSN: 1975-7220

Hydrogen evolving electrode with low Pt loading fabricated by repeated pulse electrodeposition

Hyunki Kim*, Junhyeong Kim*, Gyeong Ho Han*, Ho Won Jang, Soo Young Kim***,†, and Sang Hyun Ahn*,†**

*School of Chemical Engineering and Material Science, Chung-Ang University, Seoul 06974, Korea
**Department of Materials Science and Engineering, Research Institute of Advanced Material, Seoul National University, Seoul 08826, Korea
***Department of Materials Science and Engineering, Korea University, 145 Anam-ro, Seongbuk-gu, Seoul 02841, Korea
(*Received 2 February 2020 • Revised 14 June 2020 • Accepted 30 June 2020*)

Abstract−Reducing the Pt loading amount in an electrode is essential for the commercialization of water electrolyzers. We report a simple method for the fabrication of a low Pt loading electrode, using an electrochemical method named self-terminated electrodeposition, at room temperature and under ambient pressure. Controlling the deposition conditions enables the quenching deposition of Pt on a C-coated gas diffusion layer by H passivation at a highly negative potential. Repeating deposition pulses facilitate the facile control of the Pt surface composition and electrochemical surface area, which significantly affects their catalytic performance for the hydrogen evolution reaction. The results presented show that the aforementioned Pt electrode can be a promising cathode for use in membrane-based water electrolyzers.

Keywords: Water Electrolysis, Gas Diffusion Electrode, Hydrogen Evolution Reaction, Self-terminated Electrodeposition, Pulse Electrodeposition

INTRODUCTION

As an alternative to fossil fuels, hydrogen produced by the electrolysis of water has been recognized as a promising candidate for the sustainable generation of energy in the near future [1]. Especially when integrated with renewable energy sources, hydrogen can be obtained without the emission of pollutants [1-4]. However, hydrogen production by such a system is more expensive than that by other conventional technology [4,5], indicating that technical development is still required. To date, conventional alkaline water electrolyzers have been employed in industry, but they exhibit a large ohmic drop, difficult scale-up, toxic electrolyte usage, and low hydrogen purity [6]. As a countermeasure, water electrolyzers with ion conducting membranes sandwiched between an anode and cathode have been recently investigated to overcome these problems [6]. Although water electrolyzers with proton exchange membranes (PEMs) have a higher hydrogen production rate than those with anion exchange membranes (AEMs) [3], the high cost, which mainly originates from the usage of noble metal catalysts owing to its acidic environment, still presents a problem [7-10]. Furthermore, optimization of the membrane electrode assembly (MEA) configuration, which significantly affects the performance of the water electrolyzer in the lower current (kinetic loss) and higher current regions (mass-transfer loss), is also required [11,12].

Over the past few decades, many strategies have been investigated to fabricate high-performance MEAs. Studies on the development of highly active catalysts have focused on synthesizing multi-component catalysts with cheaper materials [13-16] and engineering their morphology to have large surface areas [7,17-19]. The effect of catalyst loading mass has also been examined to determine its lower limit for the reasonable performance of an electrolyzer [8,20]. Meanwhile, recent reports have emphasized the significant role of the MEA fabrication procedure [12,21]. As observed from the literature, MEAs prepared using the catalyst coated substrate (CCS) method exhibit higher performance than those prepared using the catalyst coated membrane (CCM) method [12,21], especially in the high current region, owing to the enhanced mass transfer of reactants and products [12]. Furthermore, *in-situ* visualization study on the inside of a PEM water electrolyzer has demonstrated that hydrogen and oxygen bubbles are generated only at the interface between the catalyst layer and membrane, thereby indicating the importance of catalyst utilization [22,23].

For the anode side where oxygen evolution reaction (OER) occurs, the Au [24], TiO_2 [25], and antimony doped tin oxide (ATO) [26] are typically used as supports, owing to their strong corrosion resistance in the operating potential window of the PEM water electrolyzer. On the other hand, at the cathode side where the hydrogen evolution reaction (HER) occurs, the potential window allows an expansive selection of support materials having high conductivity such as carbon [27], copper foam [28], and copper nanowire [29]. The Pt catalysts are deposited using magnetron sputtering [30,31] and atomic layer deposition [32,33], and their loading amount is controlled. Although these methods facilitate precise mass control in the low catalyst loading range, they require complicated and highly priced equipment to maintain high vacuum and temperature conditions. On the other hand, self-terminated electrodeposition (SED) enables the facile fabrication of ultra-low Pt loading electrode without complicated equipment under room temperature and atmo-

†To whom correspondence should be addressed.
E-mail: shahn@cau.ac.kr, sooyoungkim@korea.ac.kr

spheric pressure. When the appropriate SED potential is applied, the Pt deposition is quenched by H adsorption with a single deposition pulse and then further repeating deposition pulses facilitates precise control of the Pt loading amount [8,34,35]. In our previous study, the Pt SED was directly conducted on carbon paper (CP) to fabricate the extremely low Pt loading cathode (21 μg/cm^2) [8]. Although an acceptable performance of the PEM water electrolyzer was achieved, the cathode structure still needs to be modified to have enlarged active sites using catalyst support.

In this study, we report the simple fabrication of a low Pt loading cathode using the Pt SED method. As a first step, the feasibility of Pt SED on C-coated CP (C/CP) was examined with electrochemical, spectroscopic, and microscopic techniques. It was confirmed that a single potential pulse having the appropriate deposition potential enabled the quenching Pt deposition on the C/CP substrate. Repeating potential pulses facilitated a gradual increase in the Pt loading amount in the cathodes, along with the increase in the electrochemical surface area (ECSA). Then, their HER catalytic activity was tested in an acidic electrolyte.

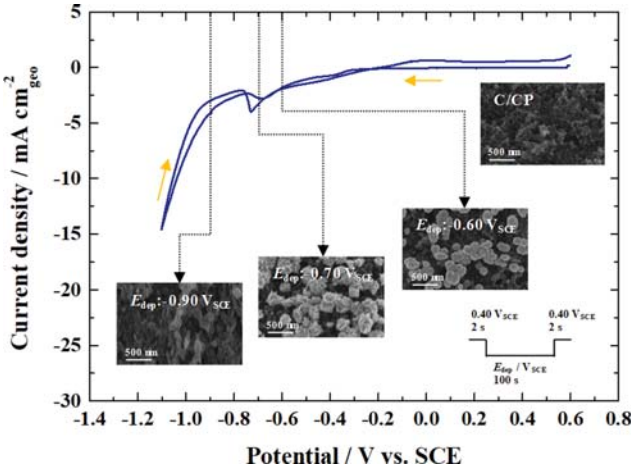

Fig. 1. CV curve of C/CP in 10 mM K_2PtCl_4 + 500 mM NaCl electrolyte at a scan rate of 10 mV/s. Insets: FESEM images of C/CP and Pt deposited C/CP.

EXPERIMENTAL

1. Preparation of C/CP Substrate

The slurry for carbon coating was composed of carbon spheres (Vulcan XC 72, Cabot), 5 wt% Nafion solution (DuPont), 18 MΩ deionized water, and isopropyl alcohol (ACS grade, Burdick & Jackson) at a weight ratio of 1.4 : 21.9 : 15.3 : 61.4. Each component was well mixed in the slurry by sonication for 30 min. Then, the spray method was used for slurry coating on the bare CP (39 BC, Sigracet). The spraying and drying were repeated until the loading amount reached 0.83 mg/cm^2.

2. Pt SED on C/CP

The electrolyte used for Pt SED consisted of 10 mM K_2PtCl_4 (99.9%, Alfa Aesar) and 500 mM NaCl (99.5%, DAEJUNG). The pH of the electrolyte was adjusted to 4.0 by adding dilute $HClO_4$ [8,34]. The Pt SED was performed in a three-electrode cell connected with a potentiostat (Autolab PGSTAT302N, Metrohm). The prepared C/CP substrate was immersed in the N_2-purged electrolyte as a working electrode. The area on which deposition occurred was measured after the Pt SED. A Pt plate was used as the counter electrode and saturated calomel electrode (SCE, KCl saturated) with a fritted junction filled with 500 mM NaCl (pH 4.0) solution was used as the reference electrode.

3. Characterization

The morphology of the catalyst was analyzed using field emission scanning electron microscopy (FESEM; SIGMA, Carl Zeiss). To examine the crystal structure and the surface composition, X-ray diffraction (XRD; New D8-Advance, BRUKER) and scanning transmission electron microscopy X-ray photoelectron spectroscopy (XPS, K-alpha+, Thermo Fisher Scientific) analyses were conducted, respectively.

4. Electrochemical Measurements

All electrochemical measurements were conducted in N_2-purged 0.5 M H_2SO_4 electrolyte at room temperature and under atmospheric pressure using a three-electrode cell connected with a potentiostat (Autolab PGSTAT302N, Metrohm). The fabricated electrodes were used as the working electrode. A Pt plate was employed as the counter electrode, whereas a reversible hydrogen electrode (RHE) with a fritted junction filled with 0.5 M H_2SO_4 (95.0%, JUNSEI) solution served as the reference electrode. To estimate the ECSA, double layer capacitance (C_{dl}) was measured using repeated cyclic voltammetry (CV) with varying scan rates. The HER activity was measured by CV in the range of 0.05~−0.50 V_{RHE} at a scan rate of 50 mV/s. As a reference, electrochemical measurement was also performed on commercial Pt foil (Alfa Aesar).

RESULTS AND DISCUSSION

A number of C spheres with diameters in the range of 100-200 nm were observed in the morphology of the C/CP substrate as shown in the inset of Fig. 1. CV at a scan rate of 10 mV/s was conducted on the bare C/CP substrate in the Pt SED electrolyte. In the negative sweep, the reduction of the Pt^{2+} ion started at −0.25 V_{SCE} and the current density gradually increased with the accelerated reduction of Pt^{2+}. The cathodic peak appeared at −0.68 V_{SCE} and then further increase in the current density resulted in the HER on the deposited Pt. In the positive sweep from −1.00 to −0.20 V_{SCE}, a similar j-V feature was observed. The anodic current represented the oxidation of the deposited Pt. The obtained CV curve was in good agreement with that in literature for Pt SED on Au [34] and CP [8], conceivably indicating the possibility of Pt SED on the C/CP substrate. To confirm this, single deposition pulse values were chosen to be 0.40 V_{SCE} (2 s), E_{dep} (100 s), and 0.40 V_{SCE} (2 s), while the E_{dep} values were chosen as −0.60 V_{SCE}, −0.70 V_{SCE}, and −0.90 V_{SCE}. For an E_{dep} of −0.60 V_{SCE}, a number of spherical Pt particles with sizes of ~500 nm were observed on the C spheres, as shown in the inset of Fig. 1, indicating that bulk electrodeposition of Pt had occurred. A similar result was obtained with an E_{dep} of −0.70 V_{SCE}, except the dendritic morphology was observed. However, with an E_{dep} of −0.90 V_{SCE}, there was no significant change in the morphology from that of the bare C/CP substrate, despite the application of a highly negative potential, thereby demonstrating

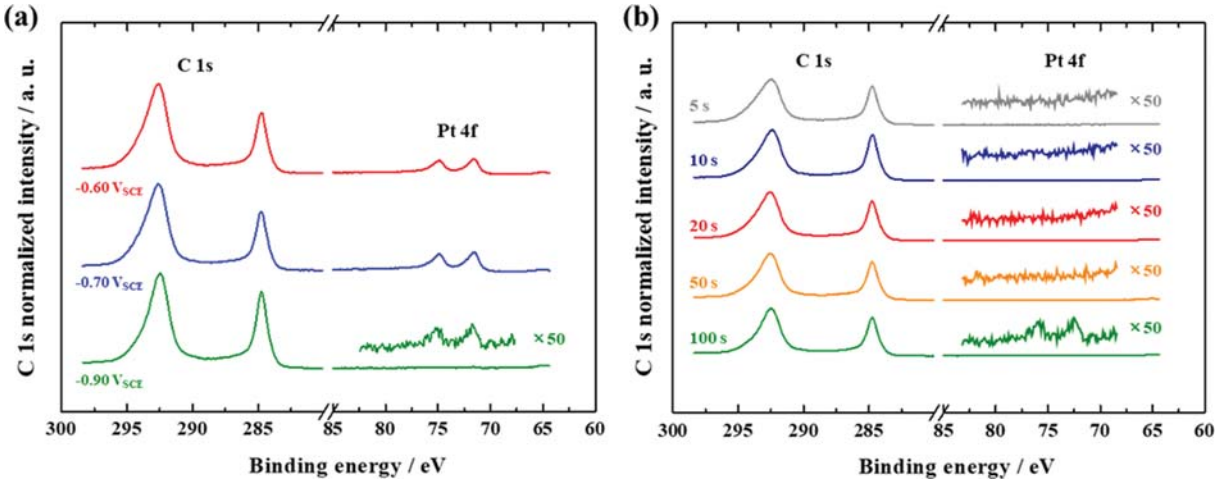

Fig. 2. XPS spectra of C 1s and Pt 4f for Pt deposited C/CP electrodes with a single potential pulse depending on (a) E_{dep} for 100 s and (b) deposition time at −0.90 V_{SCE}.

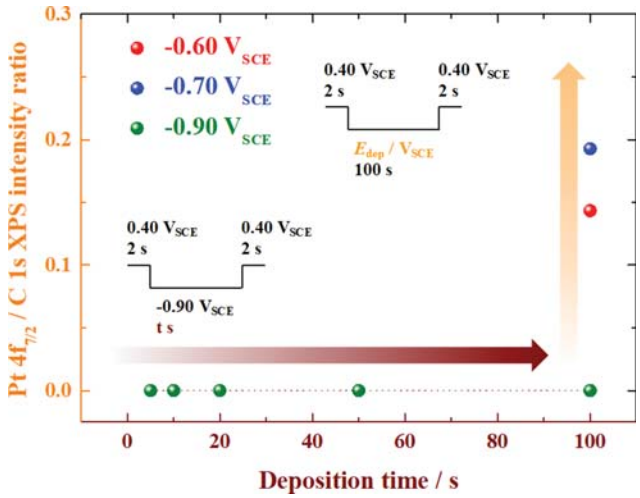

Fig. 3. Intensity ratio of the Pt $4f_{7/2}$ peak to the C 1s peak with respect to E_{dep} and deposition time.

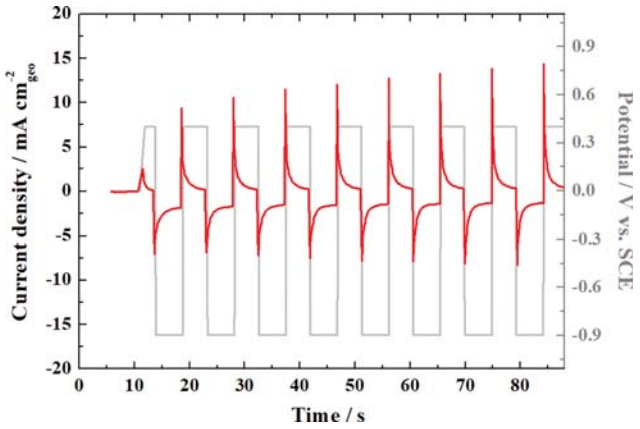

Fig. 4. Transient current as a function of time during the Pt SED potential pulses on C/CP.

the feasibility of Pt SED on the C/CP substrate.

To investigate the surface composition, XPS analysis was conducted on the three electrodes deposited at different E_{dep} values as shown in Fig. 2(a). The XPS spectra were normalized by the C 1s peak intensity at 284.8 eV. When the E_{dep} values were −0.60 and −0.70 V_{SCE}, obvious Pt 4f peaks were observed. On the other hand, Pt 4f peaks were barely seen when the E_{dep} was −0.90 V_{SCE}. However, the spectra expanded by 50 times showed the Pt 4f peak, thereby indicating the presence of Pt on the C/CP substrate. Similar results were obtained for the XPS spectra of the electrodes prepared at an E_{dep} of −0.90 V_{SCE} with varying deposition times (Fig. 2(b)). From the XPS spectra, the Pt $4f_{7/2}$/C 1s peak ratios were summarized as a function of E_{dep} and deposition time as demonstrated in Fig. 3. The ratios were significantly affected by E_{dep} at a constant deposition time of 100 s, whereas the ratios were maintained at a negligible value range, regardless of deposition time, at an E_{dep} of −0.90 V_{SCE}, indicating that the further reduction of Pt^{2+} ion was completely inhibited by H passivation [8].

Based on the aforementioned results, repetition of the potential pulse between 0.40 V_{SCE} (2 s) and −0.90 V_{SCE} (5 s) was used to increase amount of Pt deposited. The stepping potential of 0.40 V_{SCE} served to remove the adsorbed H on Pt surface, required to be reactivated for following E_{dep} [34]. Fig. 4 demonstrates the first eight representative potential pulses and the corresponding transient current. At −0.90 V_{SCE} for each pulse, the initial charging current increased gradually, whereas the final saturation current was almost constant. Similar features were obtained with anodic currents at 0.40 V_{SCE} for each pulse. The gradually increasing charging current indicated the continuous growth of Pt deposits. The electrodes obtained after multiple deposition pulses were named Pt#/C/CP (#: number of pulses deposition).

Fig. 5 shows the FESEM images of the C/CP substrate (Fig. 5(a)) and Pt#/C/CP electrode (Fig. 5(b)-(d)). For the Pt1/C/CP, it appeared that there was no morphological change, compared with the bare C/CP substrate. However, sparsely distributed small Pt nanoparticles appeared with the Pt5/C/CP. As the deposition pulse increased to 20, their particle density increased evidently without a change in size.

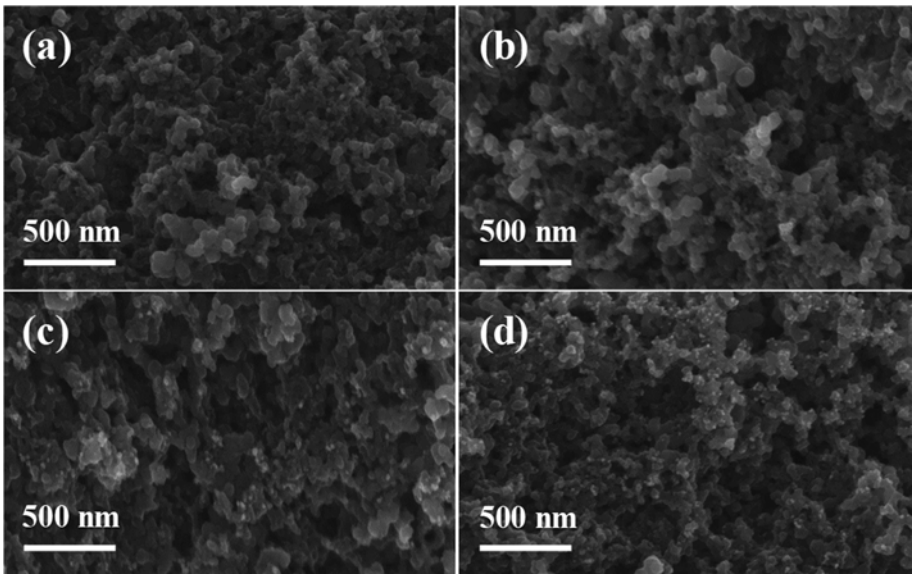

Fig. 5. FESEM images of the C/CP substrate and Pt#/C/CP electrodes: (a) C/CP, (b) Pt1/C/CP, (c) Pt5/C/CP and (d) Pt20/C/CP.

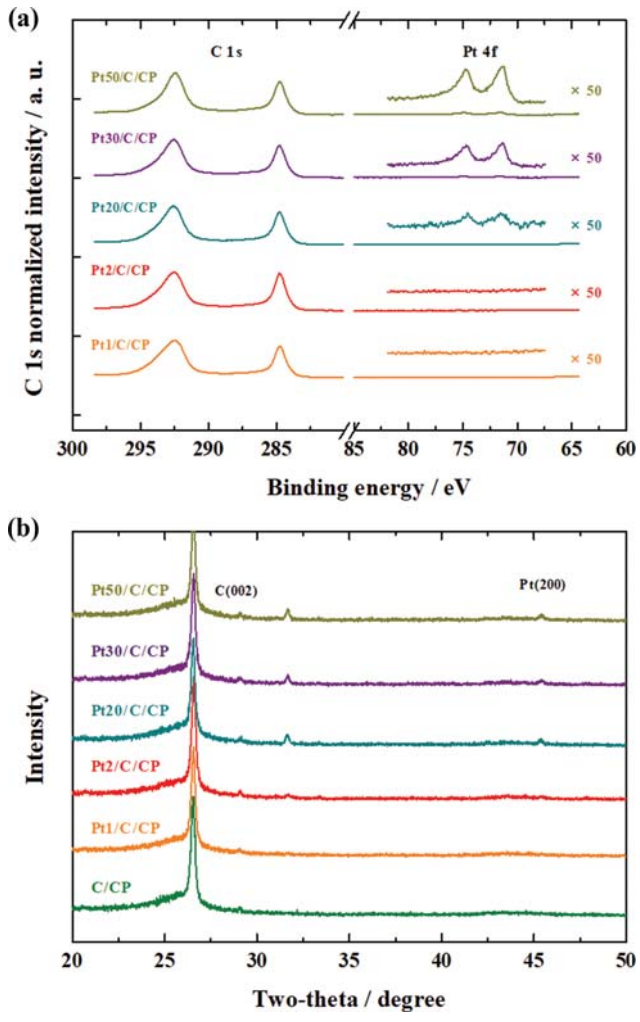

Fig. 6. (a) XPS spectra of C 1s and Pt 4f for Pt#/C/CP electrodes. (b) XRD patterns for the C/CP substrate and Pt#/C/CP electrodes.

The gradual increase of the amount of Pt as a function of the number of deposition pulses was also confirmed by XPS analysis as shown in Fig. 6(a). The XPS spectra were normalized using the C 1s peaks. For all samples, the Pt 4f peaks were mostly negligible compared with the C 1s peaks. However, in the expanded XPS spectra, the intensity of the Pt 4f peak increased gradually with the increase in the number of deposition pulses from 20 to 50. The XRD patterns of the C/CP substrate and Pt#/C/CP electrode showed similar results (Fig. 6(b)). For the substrate, a sharp C (002) peak appeared at 26.4°, mainly originating from carbon spheres. The Pt peaks were barely observed, except the Pt (200) peak at 45.3°, on increasing the number of deposition pulses from 20 to 50; this was consistent with the XPS result. XPS and XRD results confirmed that very a low amount of Pt was deposited on the Pt#/C/CP electrode, despite the number of deposition pulses being increased to 50.

To estimate the ECSA, C_{dl} of Pt#/C/CP was measured using repeated CV in a 0.5 M H_2SO_4 electrolyte by varying the scan rate (Fig. S1 and S2). The results are summarized as a function of the number of deposition pulses (Fig. 7(a)). The C_{dl} of Pt1~5/C/CP showed values similar to that of bare C/CP, indicating no significant change of ECSA. However, when the number of deposition pulses was increased from 5 to 30, the C_{dl} value increased linearly, indicating the enlargement of Pt ECSA. Then, the C_{dl} of Pt50/C/CP showed similar values to that of Pt30/C/CP, conceivably showing the agglomeration of Pt nanoparticles at a higher number of deposition pulses.

Fig. 7(b) shows the linear sweep voltammetry (LSV) curve of C/CP and Pt#/C/CP in 0.5 M H_2SO_4 at a scan rate of 50 mV/s. The bare C/CP exhibits negligible current in the entire potential range. On the other hand, compared to this, the Pt1/C/CP demonstrates a small but obvious current density for HER. This is evidence for Pt formation after one pulse deposition even though the Pt peaks were not observed in XPS (Fig. 6(a)) and XRD (Fig. 6(b)). The HER current density gradually increased on increasing the number of deposition pulses from 1 to 30 and was higher than that of com-

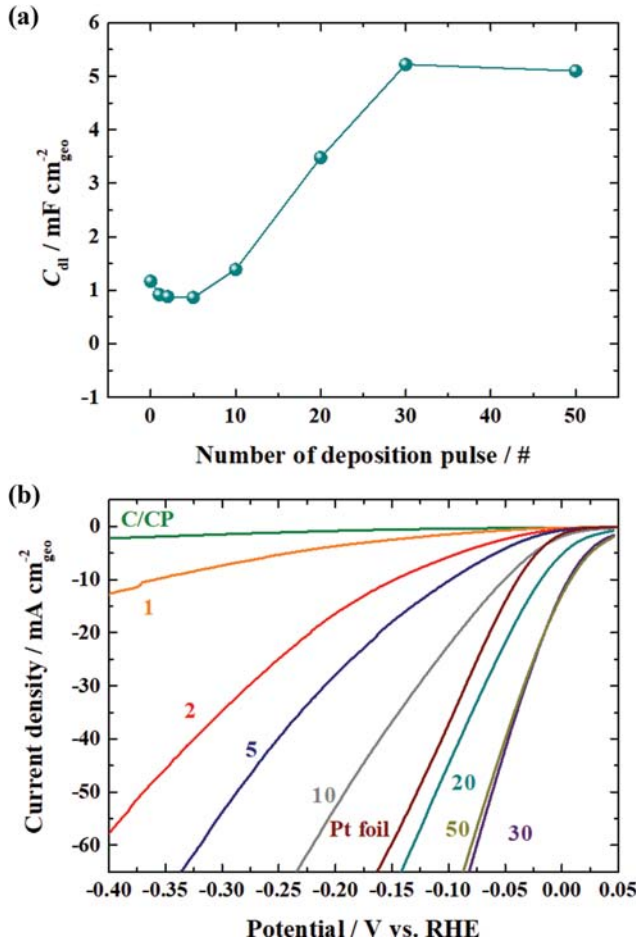

Fig. 7. (a) C_{dl} of Pt#/C/CP as a function of the number of deposition pulses. (b) CV curves for HER activity test in 0.5 M H_2SO_4 at a scan rate of 50 mV/s.

mercial Pt foil after 20 pulses. The Pt50/C/CP showed similar activity with Pt30/C/CP. The results are consistent with the trend of C_{dl}, indicating the importance of ECSA in HER activity for single element catalysts.

CONCLUSION

We have demonstrated a facile method to fabricate a low Pt loading electrode and confirmed that the quenching Pt deposition by H passivation on the C/CP substrate is significantly affected by the E_{dep} of the deposition pulse. After using the optimized conditions for Pt SED, repeating the deposition pulse facilitated the simple control of the Pt surface composition. The HER activity increased gradually with the increase in the number of deposition pulses, which showed similar tendency with the C_{dl} measurement. This simply fabricated electrode with low Pt loading is a promising cathode for use in highly efficient PEM water electrolyzers.

ACKNOWLEDGEMENTS

This research was supported by Korea Electric Power Corporation (Grant number: R18XA06-27) and by the Chung-Ang University Graduate Research Scholarship in 2019.

SUPPORTING INFORMATION

Additional information as noted in the text. This information is available via the Internet at http://www.springer.com/chemistry/journal/11814.

REFERENCES

1. J. A. Turner, *Science*, **305**, 972 (2004).
2. S. E. Hosseini and M. A. J. R. Wahid, *Renew. Sust. Energ. Rev.*, **57**, 850 (2016).
3. C. Acar and I. Dincer, *Int. J. Hydrog. Energy*, **39**, 1 (2014).
4. B. Lee, H. Chae, N. H. Choi, C. Moon, S. Moon and H. Lim, *Int. J. Hydrogen Energy*, **42**, 6462 (2017).
5. M. Voldsund, K. Jordal and R. Anantharaman, *Int. J. Hydrogen Energy*, **41**, 4969 (2016).
6. J. D. Holladay, J. Hu, D. L. King and Y. Wang, *Catal. Today*, **139**, 244 (2009).
7. J. E. Park, S. Kim. O.-H. Kim, C.-Y. Ahn, M.-J. Kim, S. Y. Kang, T. I. Jeon, J.-G. Shime, D. W. Lee, J. H. Lee, Y.-H. Cho and Y.-E. Sung, *Nano Energy*, **58**, 158 (2019).
8. H. Kim, S. Choe, H. Park, J. H. Jang, S. H. Ahn and S.-K. Kim, *Nanoscale*, **9**, 190545 (2017).
9. B.-S. Lee, S. H. Ahn, H.-Y. Park, I. Choi, S. J. Yoo, H.-J. Kim, D. Henkensmeier, J. Y. Kim, S. Park, S. W. Nam, H.-Y. Lee and J. H. Jang, *Appl. Catal. B-Environ.*, **179**, 285 (2015).
10. S. Choe, B.-S. Lee, M. K. Cho, H.-J. Kim, D. Henkensmeier, S. J. Yoo, J. Y. Kim, S. Y. Lee, H. S. Park and J. H. Jang, *Appl. Catal. B-Environ.*, **226**, 289 (2018).
11. J. Kim, J. Kim, H. Kim and S. H. Ahn, *ACS Appl. Mater. Interfaces*, **11**, 330774 (2019).
12. M. Bühler, P. Holzapfel, D. McLaughlin and S. Thiele, *J. Electrochem. Soc.*, **166**, F1070 (2019).
13. Q. Chen, Z. Cao, G. Du, Q. Kuang, J. Huang, Z. Xie and L. Zheng, *Nano Energy*, **39**, 582 (2017).
14. X. Cao, Y. Han, C. Gao, Y. Xu, X. Huang, M. Willander and N. Wang, *Nano Energy*, **9**, 301 (2014).
15. Y. Shi and B. Zhang, *Chem. Soc. Rev.*, **45**, 1529 (2016).
16. Y. Guo, T. Park, J. W. Yi, J. Henzie, J. Kim, Z. Wang, B. Jiang, Y. Bando, Y. Sugahara, J. Tang and Y. Yamauchi, *Adv. Mater.*, **31**, 1807134 (2019).
17. D. V. Esposito, S. T. Hunt, A. L. Stottlemyer, K. D. Dobson, B. E. McCandless, R. W. Birkmire and J. G. Chen, *Angew. Chem. Int. Ed.*, **49**, 9859 (2010).
18. D. V. Esposito, S. T. Hunt, Y. C. Kimmel and J. G. Chen, *J. Am. Chem. Soc.*, **134**, 3025 (2012).
19. Y. Pi, Q. Shao, X. Zhu and X. Huang, *ACS Nano*, **12**, 7371 (2018).
20. Y. Wang, X. Yu, G. Liu, X. Zhu, R. Xu, M. Ji, Y. Ma and L. Ma, *Adv. Sustainable Syst.*, **3**, 1900026 (2019).
21. M. Bühler, F. Hegge, P. Holzapfel, M. Bierling, M. Suermann, S. Vierrath and S. Thiele, *J. Mater. Chem. A*, **7**, 26984 (2019).
22. J. Mo, Z. Kang, S. T. Retterer, D. A. Cullen, T. J. Toops, J. B. Green, M. M. Mench and F.-Y. Zhang, *Sci. Adv.*, **2**, e1600690 (2016).
23. Z. Kang, G. Yang, J. Mo, Y. Li, S. Yu, D. A. Cullen, S. T. Retterer,

T. J. Toops, G. Bender, B. S. Pivovar, J. B. Green and F.-Y. Zhang, *Nano Energy*, **47**, 434 (2018).
24. Y. Zeng, X. Guo, Z. Shao, H. Yu, W. Song, Z. Wang, H. Zhang and B. Yi, *J. Power Sources*, **342**, 947 (2017).
25. J. Cheng, J. Yang, S. Kitano, G. Juhasz, M. Higashi, M. Sadakiyo, K. Kato, S. Yoshioka, T. Sugiyama, M. Yamauchi and N. Nakashima, *ACS Catal.*, **9**, 6974 (2019).
26. F. Claudel, L. Dubau, G. Berthome, L. Sola-Hernandez, C. Beauger, L. Piccolo and F. Maillard, *ACS Catal.*, **9**, 4688 (2019).
27. A. A. Fedotov, S. A. Grigoriev, P. Millet and V. N. Fateev, *Int. J. Hydrogen Energy*, **39**, 8568 (2013).
28. J. Kim, H. Kim, J. Kim, J. H. Kim and S. H. Ahn, *J. Alloy Compd.*, **807**, 1448813 (2019).
29. H. Kim, H. Park, D.-K. Kim, S. Oh, I. Choi and S.-K. Kim, *ACS Sust. Chem. Eng.*, **7**, 8265 (2019).
30. S. Hussain, H. Erikson, N. Kongi, A. Tarre, P. Ritslaid, M. Rähn, L. Matisen, M. Merisalu, V. Sammelselg and K. Tammeveski, *Int. J. Hydrogen Energy*, **43**, 4967 (2018).
31. H. Wang, M. Zhang, F. Cheng and C. Xu, *Int. J. Electrochem. Sci.*, **3**, 946 (2008).
32. J. Li, W. Liu, J. Wang, I. Rozen, S. He, C. Chen, H. G. Kim, H.-J. Lee, H.-B.-R. Lee, S.-H. Kwon, T. Li, L. Li, J. Wang and Y. Mei, *Adv. Funct. Mater.*, **27**, 1700598 (2017).
33. I. J. Hsu, Y. C. Kimmel, X. Jiang, B. G. Willis and J. G. Chen, *Chem. Commun.*, **48**, 1063 (2012).
34. Y. Liu, D. Gokcen, U. Bertocci and T. P. Moffat, *Science*, **388**, 1327 (2012).
35. S. H. Ahn, Y. Liu and T. P. Moffat, *ACS Catal.*, **5**, 2124 (2015).

Supporting Information

Hydrogen evolving electrode with low Pt loading fabricated by repeated pulse electrodeposition

Hyunki Kim*, Junhyeong Kim*, Gyeong Ho Han*, Ho Won Jang, Soo Young Kim***,†, and Sang Hyun Ahn*,†**

*School of Chemical Engineering and Material Science, Chung-Ang University, Seoul 06974, Korea
**Department of Materials Science and Engineering, Research Institute of Advanced Material, Seoul National University, Seoul 08826, Korea
***Department of Materials Science and Engineering, Korea University, 145 Anam-ro, Seongbuk-gu, Seoul 02841, Korea
(*Received 2 February 2020 • Revised 14 June 2020 • Accepted 30 June 2020*)

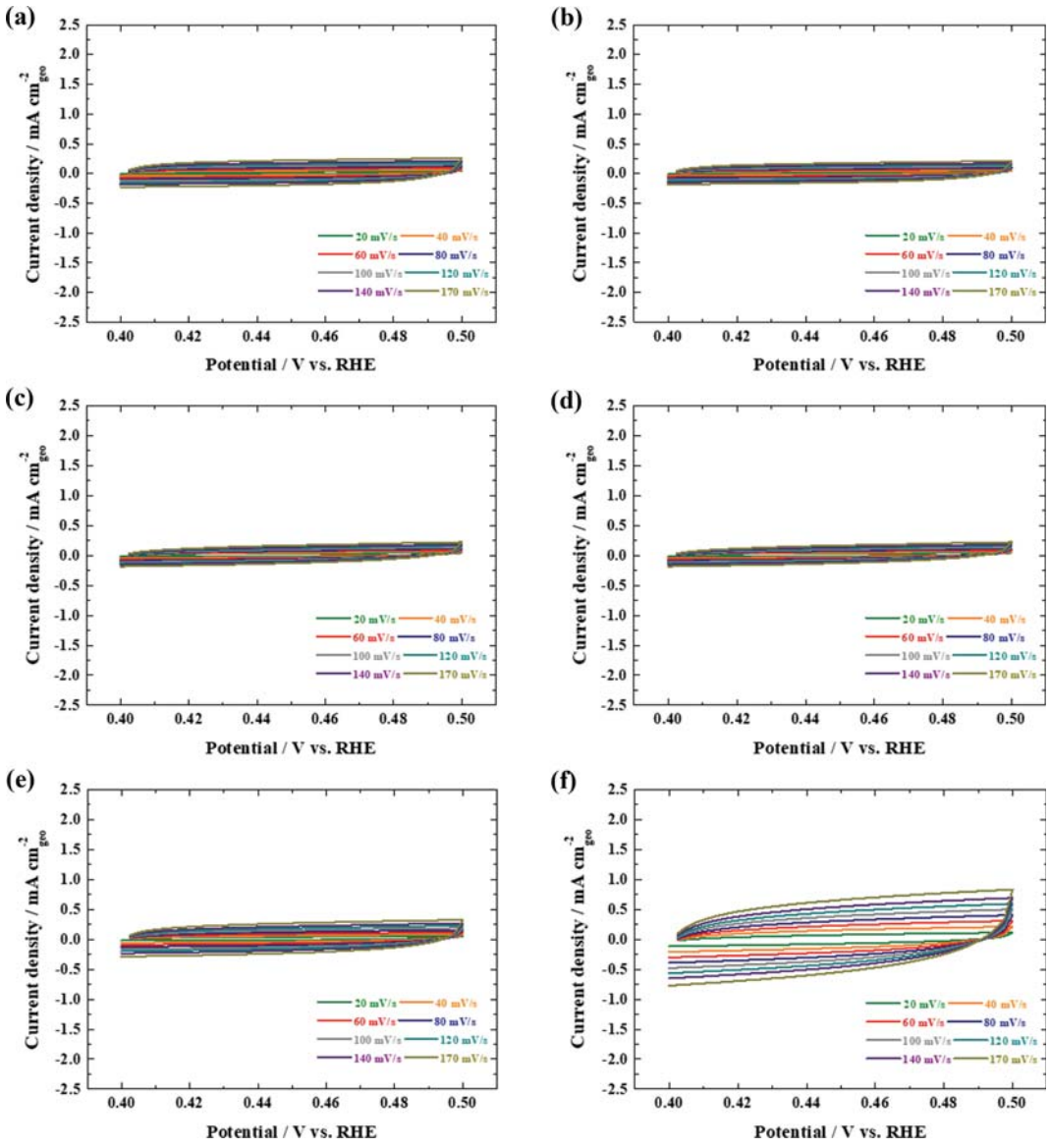

Fig. S1. CV curves at various scan rate in 0.5 M H_2SO_4 electrolyte for (a) C/CP, (b) Pt1/C/CP, (c) Pt2/C/CP, (d) Pt5/C/CP, (e) Pt10/C/CP, (f) Pt20/C/CP, (g) Pt30/C/CP, and (h) Pt50/C/CP.

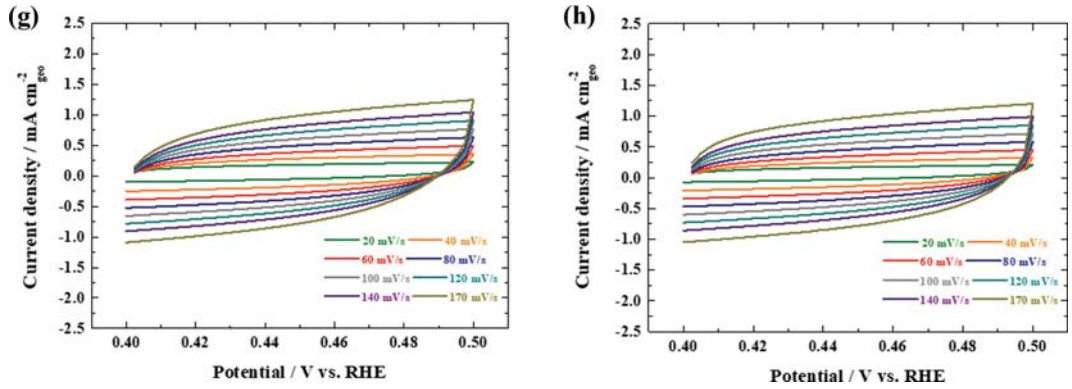

Fig. S1. Continued.

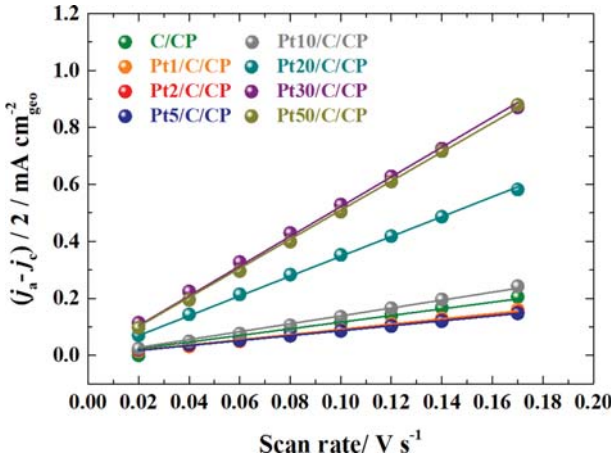

Fig. S2. C_{dl} measurement on C/CP substrate and Pt#/C/CP electrodes.